KSCE Journal of Civil Engineering (2021) 25(9):3458-3476
DOI 10.1007/s12205-021-2092-4

pISSN 1226-7988, eISSN 1976-3808
www.springer.com/12205

Structural Engineering

Calculation of Deflection and Stress of Assembled Concrete Composite Beams under Shrinkage and Creep and Its Application in Member Design Optimization

Yan Fang[a,b], **Jianghong Mao**[b,c,d], **Yixue Zhang**[a,b], **Weiliang Jin**[a,b], **Diwei Tang**[a,b], **and Jun Zhang**[b,c]

[a]*Institute of Structural Engineering, Zhejiang University, Hangzhou 310058, China*
[b]*Institute of Structural and Bridge Engineering, Ningbo Tech University, Ningbo 315000, China*
[c]*Ningbo Research Institute, Zhejiang University, Ningbo 315000, China*
[d]*College of Architecture & Environment, Sichuan University, Chengdu 610065, China*

ARTICLE HISTORY

Received 24 November 2020
Revised 1 March 2021
Accepted 14 April 2021
Published Online 18 June 2021

KEYWORDS

Assembled composite beams
Shrinkage
Creep
Calculation method
Numerical simulation
Sensitivity analysis
Design optimization

ABSTRACT

There are a large number of concrete bonding interfaces in assembled concrete structures. Moreover, the problems of deformation and coordination at the interfaces lead to weak bonding under shrinkage and creep. The theoretical methods and analytical solutions for the long-term performance of composite structures in recent literatures are relatively complicated for the review or optimization in the design stage. Hence, a method for calculating the mid-span deflection of and the cross-sectional stress on composite beams under shrinkage and creep was developed based on the average curvature method. The calculation method was then verified by the experiments and the numerical simulations. Further, factors affecting the deflection of and the stress on the assembled concrete composite beams, including the loading age, the reinforcement ratio, the section dimensions, and the surface area in contact with the atmosphere were analyzed by using the developed method. The results revealed that the adjustment of the section dimensions and the loading time is the effective optimization approach. A framework for review or optimization of composite concrete beams based on the sensitivity analysis is proposed and a case study is carried out. The results of this work can helpfully be used to control the risk of additional deflections or cracking during the long-term operation of buildings.

1. Introduction

Interfaces, the connection between two different components in composite members, exist widely in all types of composite structures (CS), including the steel–concrete composite structure (SCCS), the timber–concrete composite structure (TCCS) (Cosenza and Pecce, 2001), the assembled concrete composite structure (ACCS) (Xue et al., 2019), and the repaired/reinforced concrete composite structure (RCCS) (Halicka, 2011). Old and new concrete interfaces are widely present in concrete structures, not only in RCCSs (Long et al., 2014) but also in new ACCSs (Xue et al., 2020). The shrinkage and creep of different materials, or rather different types of concrete, cause various engineering problems such as slips and cracks (Cyron et al., 2019; Orta and Bartlett, 2020).

An assembled concrete composite structure is a building structure the concrete components of which, namely beams, columns, wall panels, and floor units, are cast either at a factory or at a fixed location on site, and the completed elements are erected and assembled in situ (Chiang et al., 2006; Hong et al., 2018; Kurama et al., 2018). This form of structure has the advantages of the high construction efficiency, the high quality of precast units, and the reduction of in situ formwork (Fan et al., 2020; Hu et al., 2020). Thus, ACCSs have been rapidly promoted and widely applied in the world (Khoo et al., 2006; Chen et al., 2012). However, there are a large number of concrete bonding interfaces in ACCSs, which are the weak parts influencing the structural performance such as flexural resistance (Gohnert, 2000; Gillum et al., 2001),

CORRESPONDENCE Jianghong Mao jhmao@nit.zju.edu.cn Institute of Structural and Bridge Engineering, Ningbo Tech University, Ningbo 315000, China; Ningbo Research Institute, Zhejiang University, Ningbo 315000, China; College of Architecture & Environment, Sichuan University, Chengdu 610065, China

shear resistance (Halicka, 2011), and durability (Huang et al., 2019b). Moreover, the additional deflections or unexpected cracking of these structures due to the different shrinkage and creep behaviors of old and new concrete are special engineering problems, the effect mechanism and the controlling method of which should receive further attention.

The effect mechanism of the additional deflections or unexpected cracking of CS has been reported in some literature (Beushausen, 2016; Lam et al., 2019). In fact, materials used in CSs have their respective shrinkage characteristics, which causes differential movement at the interface; this mechanism is considered as an important reason for the above problems (Lam et al., 2019). It has been reported that the flexural deformation of and the tensile stress on concrete due to the restrained shrinkage (Khan et al., 2017; Zhu et al., 2020) can result in cracking if the tensile strength of the concrete is exceeded. Although the effect mechanisms of various types of composite structures are similar, there are a number of obvious differences between ACCSs and the other CSs, leading to some new issues.

Firstly, the shrinkage and creep behaviors of the materials on both sides of the interface of ACCSs differ from those of other composite structures. For example, the steel in SCCSs or the timber in TCCSs hardly shrinks and creeps. Moreover, the loading age of the old concrete of RCCSs is extremely large, and shrinkage has already progressed in the concrete matrix (Jung et al., 2017), which implies that the shrinkage and creep of old concrete are almost developed in RCCSs. Nonetheless, the loading age of the old concrete of ACCSs is much smaller, so the shrinkage and creep of the new and old concrete need to be considered simultaneously. The loading age of concrete is an important factor influencing the behavior of creep and is considered in creep prediction codes (ACI Committee 209, 1982; CEB, 1992) or empirical models (Bažant and Bweja, 1995; Gardner and Lockman, 2001). Therefore, the additional deflection of and the stress on composite structures can be apparently different (Huang et al., 2019a).

Secondly, compared with SCCSs and TCCSs, ACCSs own a simple section form and material properties (Xue et al., 2019). Thus, theoretical formulations and numerical solutions can be proposed for calculating the deflection of and the stress on ACCSs under shrinkage and creep. The finite element method (FEM) is commonly used for analyzing the long-term performance of composite structures (Erkmen and Bradford, 2011; Si and Au, 2011; Liu et al., 2012; Liu et al., 2016). Although the deflection of and the stress on composite structures under shrinkage and creep can be obtained by the FEM (Ban et al., 2015; Han et al., 2019; Morenoa et al., 2019; Martinelli, 2021), it is relatively complicated for practical structure design or optimization. Therefore, it is necessary to propose a theoretical calculation method for design and optimization. Some analytical models of the mechanical performance of composite beams have been reported in the related literature (Schnabl et al., 2007; Ecsedi and Baksa, 2016; Cas et al., 2018; Magnucki et al., 2020). Further, a number of improved models considering the long-term effect of the interface of SCCSs have been proposed (Ranzi and Bradford, 2006; Chen and Yossef, 2016; Bertagnoli et al., 2017); the interface effect is only taken into account for the concrete part of SCCSs. However, since both concrete parts of ACCSs are under the sustained and time-dependent interface effect, it is necessary to develop a special theoretical model of ACCSs.

The design process of the components of ACCSs differs from that of normal reinforced concrete because the shrinkage and creep give rise to the risk of the additional deflection and unexpected cracking of ACCSs. In addition to section design based on the ultimate limit state, the section review or optimization considering shrinkage and creep should be added during checking the traditional serviceability limit state. There are a number of factors which are beneficial to the reduction the additional deflection of and the stress on the interface of ACCSs. The factors with the function of changing the shrinkage and creep behavior can be considered as the optimizable parameters. They include the loading age, the reinforcement ratio, the section dimensions, and the surface area in contact with the atmosphere. Thus, the additional deflection or unexpected cracking can be controlled during the design stage of ACCSs.

Based on the average curvature method (Chen, 1981), this paper develops a theoretical formula for calculating the additional mid-span deflection of and the section stress on assembled concrete composite beams. The differential shrinkage and creep results in additional deflections and stresses, and its time-dependent creep effect is considered in the calculation. The accuracy of the theoretical model is then verified by the experimentation and the numerical simulation. Furthermore, a sensitivity analysis using the developed theoretical model is conducted to examine the effect mechanisms of the different parameters, and the influence of each parameter on the mid-span deflection, the section stress, and possible failure time is studied. Finally, a design optimization frame is proposed to control the additional deflection of and the stress on the interface of ACCBs. The results of this work can provide a scientific basis and a guidance for the design of assembled concrete composite beams considering shrinkage and creep.

2. Theoretical Calculation Method

2.1 Deflection Calculation Method

2.1.1 Fundamental Hypotheses

The separated precast beams and slabs are combined with cast-in-place concrete in an assembled structure. A T-section is then formed by the precast members and the cast-in-place members. According to the calculation width of the flange in a T-section beam given by Code GB 50010 (2010), an assembled concrete composite beam (ACCB) with a typical cross-section is proposed. The typical section of the ACCB is shown in Fig. 1(a). The CEB–FIP models and the ACI models are widely used to calculate the shrinkage and creep in practical applications respectively; in this paper, the CEB–FIP 90 model (CEB, 1992) is adopted in the

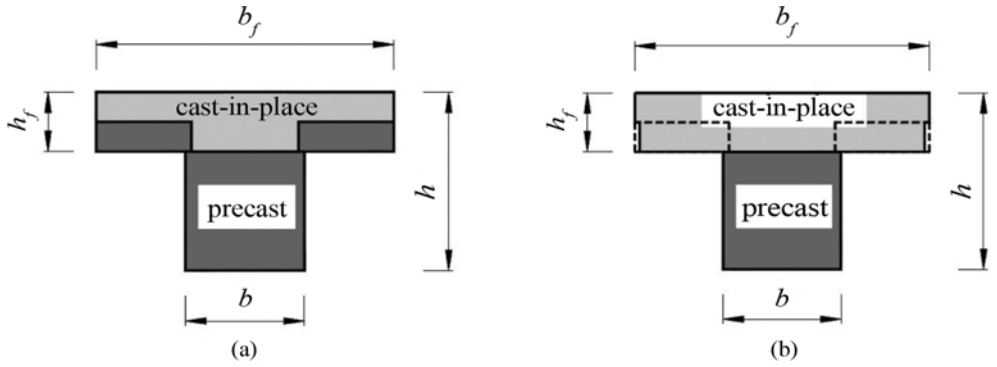

Fig. 1. The Typical Cross-Section of the ACCB: (a) Before Replacement, (b) After Replacement

theoretical calculation. The following hypotheses are introduced while calculating the deflection of the ACCB:

1. The ACCB is in the elastic working stage;
2. Steel bars in the ACCB are converted into the equivalent concrete. The gravity axis of the section and the force on it remain unchanged during the conversion;
3. The stiffness of the flange of the section is far lower than that of the web. The impact of the shrinkage and creep of the precast concrete on the deflection of the ACCB can be ignored. Therefore, the precast concrete (PRC) at the flange is replaced with the cast-in-place concrete (CIC). The replaced section is shown in Fig. 1(b).

2.1.2 Deflection Composition

The deflection of the ACCB (w) increases with time under shrinkage and creep, and it can be expressed by

$$w = w_0 + w_1 + w_2 , \tag{1}$$

where w_0 is the initial deflection of the ACCB caused by the load, w_1 represents the variation in the deflection of the ACCB under creep, and w_2 indicates the deflection variation of the ACCB caused by the differential shrinkage and creep (DSC) at the interface between the PRC and CIC.

2.1.3 Variation in Deflection of the ACCB under Creep

The development of the deflection of the ACCB is shown in Fig. 2. An initial deflection of the ACCB (w_0) is produced by a load, and it increases under the creep. Before compositing the PRC and the CIC, the deflections of the PRC and the CIC are $\varphi_p w_0$ and $\varphi_c w_0$, respectively. When the PRC and the CIC are composited, the final deflection of the ACCB after deformation coordination is w_1. The deformation of the PRC and the CIC is inversely proportional to the bending stiffness. Therefore, the deflection of the PRC after being composited (w_p) is expressed in

$$w_p = \frac{E_1 I_1}{E_1 I_1 + E_2 I_2}\left(\varphi_c - \varphi_p\right) w_0 , \tag{2}$$

where φ_p and φ_c are the creep coefficient of the PRC and the CIC, respectively. $E_1 I_1$ and $E_2 I_2$ represent the bending stiffness of the CIC and the PRC after equivalent substitution, respectively.

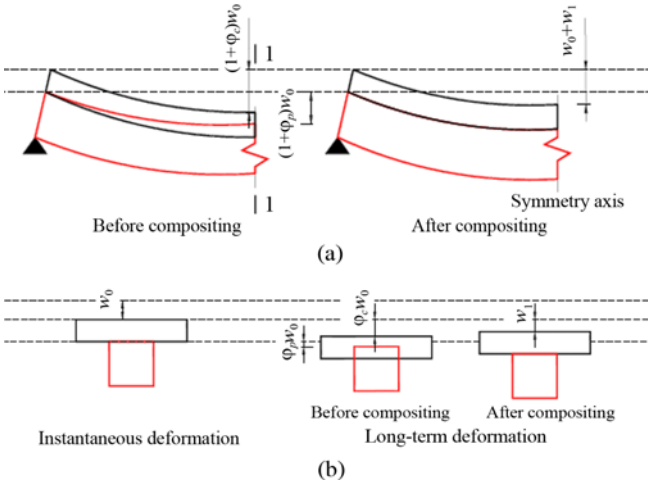

Fig. 2. The Evolution Process of the Deflection of the ACCB: (a) Deflection of the PRC and the CIC under Creep, (b) The Evolution Process of the Deflection of Section 1–1

The deflection of an ACCB (w_1) while considering creep is expressed through

$$w_1 = \left(\frac{E_2 I_2}{E_1 I_1 + E_2 I_2}\varphi_p + \frac{E_1 I_1}{E_1 I_1 + E_2 I_2}\varphi_c\right) w_0 . \tag{3}$$

2.1.4 Deflection of the ACCB Caused by Differential Shrinkage and Creep

The difference in the strains of the PRC and the CIC is defined as the differential shrinkage and creep (DSC), which is denoted by D, as shown in Fig. 3(a). The DSC is caused by the differential movement between concrete with different strength grade and the loading age. According to the deformation coordination, the deformation of PRC and the CIC at the composite interface should be identical. Thus, a bending deflection of the ACCB occurs as shown in Fig. 3(b), where θ is the mid-span curvature, and shear stress exists at the composite interface between the PRC and the CIC. The average curvature method proposed by Chen (1981) supposes that the curvature caused by the DSC is uniformly distributed along the beam when calculating the additional deflection of the ACCB caused by the DSC, and the

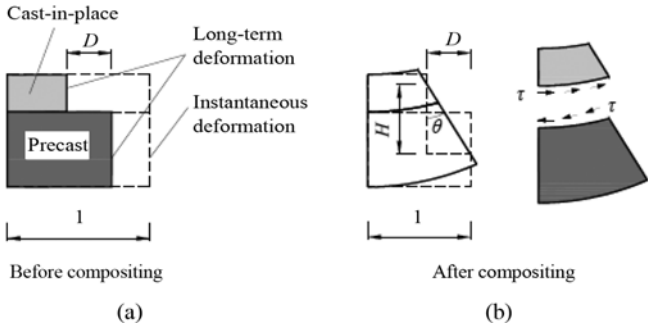

Fig. 3. The Differential Shrinkage and Creep (D) and the Curvature (θ): (a) Before Compositing, (b) After Compositing

calculation data are close to the experimental results presented in the paper. According to the relationship between the deflection of the beam and the mid-span curvature, the deflection caused by D and θ at the mid-span of the ACCB is given by

$$w_2 = (\alpha\theta_c + 0.125\theta_s)L^2 , \tag{4}$$

where α is related to the load form, which is 23/216 under a four-point loading; L is the span; θ_c and θ_s indicate the mid-span curvatures caused by the DSC and are calculated by

$$\theta_c = D_c / H , \tag{5}$$

$$\theta_s = D_s / H , \tag{6}$$

where H is the distance between the neutral axis of the differential stresses on the PRC and the CIC and can be calculated by the average curvature method; D_c and D_s are the mid-span differential creep and differential shrinkage respectively and are defined as

$$D_c = (\varphi_{cc}(t) - \varphi_{pc}(t))\varepsilon_0 , \tag{7}$$

$$D_s = (\varepsilon_{csh}(t) - \varepsilon_{csh}(t_0)) - (\varepsilon_{psh}(t) - \varepsilon_{psh}(t_0)) , \tag{8}$$

where ε_0 is the initial strain at the composite interface; $\varphi_{cc}(t)$ and $\varphi_{pc}(t)$ represent the creep coefficient of the CIC and the PRC, respectively; $\varepsilon_{csh}(t_0)$ and $\varepsilon_{csh}(t)$ indicate the shrinkage strain of the CIC at the loading moment and at the calculation moment, respectively; $\varepsilon_{psh}(t_0)$ and $\varepsilon_{psh}(t)$ stand for the shrinkage strain of the PRC at the loading moment and at the calculation moment, respectively.

2.1.5 Effect of Creep on Deflection Caused by DSC

Although both the PRC and the CIC undergo long-term creep after being composited, the effect of the interactions between these two parts under long-term creep was not considered while calculating w_2. The influence of creep on w_2 can be divided into two parts: the first one is a reduction in the deflection of the ACCB because the long-term creep decreases the DSC, and the second part is an increase in the deflection of the ACCB because the long-term creep enlarges the curvature.

Because of the creep effect of the interaction between the two parts, the DSC under long-term creep is smaller than the one recorded before compositing the beam and is calculated by

$$D = D_c + D_s . \tag{9}$$

The actual value of the DSC after compositing the beam is denoted by d. The strains on the bottom of the CIC (μ_c) and on the top of the PRC (μ_p) are defined as

$$\mu_c = ad , \tag{10}$$

$$\mu_p = bd , \tag{11}$$

where a and b are related to the stiffness of the section and can be calculated as follows:

$$a = \frac{E_2 I_2}{E_1 I_1 + E_2 I_2} , \tag{12}$$

$$b = \frac{E_1 I_1}{E_1 I_1 + E_2 I_2} . \tag{13}$$

During the period of time Δt, the variation in d under creep is given by

$$\Delta d = \mu_p \Delta\varphi_p + \mu_c \Delta\varphi_c . \tag{14}$$

Therefore, d and D have the following relationship

$$d = D - \int (ad\,\mathrm{d}\varphi_c + bd\,\mathrm{d}\varphi_p) . \tag{15}$$

According to Eq. (4), the deflection caused by the actual DSC is expressed by

$$w_d(t) = kd(t)L^2 / H , \tag{16}$$

where the value of k ranges from α to 0.125 and is related to the proportions of D_c and D_s in D. It is set at 0.125 in this work since the differential creep is much smaller than the differential shrinkage, that is, $D_c \ll D_s$.

The reduction in the deflection of the ACCB considering the long-term creep (the first part of the effect) can be obtained by substituting Eq. (14) into Eq. (16)

$$\begin{aligned} \Delta w_2^- &= k(\mu_p \Delta\varphi_p + \mu_c \Delta\varphi_c)L^2 / H \\ &= k(bd(t)\Delta\varphi_p + ad(t)\Delta\varphi_c)L^2 / H \\ &= (b\Delta\varphi_p + a\Delta\varphi_c)w_d(t) . \end{aligned} \tag{17}$$

The increment in the deflection of the ACCB (the second part of the effect) during Δt is given by

$$\Delta w_2^+ = \left(\frac{E_2 I_2}{E_1 I_1 + E_2 I_2}\Delta\varphi_p + \frac{E_1 I_1}{E_1 I_1 + E_2 I_2}\Delta\varphi_c\right) w_d(t) . \tag{18}$$

Therefore, the variation in w_2 considering Δw_2^- and Δw_2^+ during Δt is defined as

$$\begin{aligned} \Delta w_2 &= \Delta w_2^+ - \Delta w_2^- \\ &= w_d(t)\left[\left(\frac{E_2 I_2}{E_1 I_1 + E_2 I_2} - \frac{E_1 I_1}{E_1 I_1 + E_2 I_2}\right)\Delta\varphi_p + \left(\frac{E_1 I_1}{E_1 I_1 + E_2 I_2} - \frac{E_2 I_2}{E_1 I_1 + E_2 I_2}\right)\Delta\varphi_c\right] \\ &= w_d(t)\frac{E_1 I_1 - E_2 I_2}{E_1 I_1 + E_2 I_2}(\Delta\varphi_c - \Delta\varphi_p) . \end{aligned} \tag{19}$$

Also, w_2 is corrected to

$$w_2 = (\alpha\theta_c + 0.125\theta_s)L^2 + \int w_d(t)\frac{E_1I_1 - E_2I_2}{E_1I_1 + E_2I_2}(\mathrm{d}\varphi_c - \mathrm{d}\varphi_p) \ . \quad (20)$$

The values of d and w_2 are calculated with the assistance of MATLAB software in this work since they can hardly be calculated directly.

2.2 Calculation Method of Cross-Sectional Stress

2.2.1 Stress Composition

The cross-sectional stress on the ACCB can be expressed in

$$\sigma = \sigma_0 + \sigma_1 + \sigma_\rho \ , \quad (21)$$

where σ_0 is the initial stress caused by loading; σ_1 represents the stress caused by the DSC at the composite interface as shown in Fig. 3; σ_ρ indicates the stress caused by the restraining effect of the steel bars on the concrete.

2.2.2 Stress Caused by DSC

The stresses on the upper and lower sections of the CIC and the PRC are given by

$$\sigma_{1cT} = \theta E_1(y_1 - y_{1T}) \ , \quad (22)$$

$$\sigma_{1cB} = \theta E_1(y_1 + y_{1B}) \ , \quad (23)$$

$$\sigma_{1pT} = -\theta E_2(y_2 + y_{2T}) \ , \quad (24)$$

$$\sigma_{1pB} = -\theta E_2(y_2 - y_{2B}) \ . \quad (25)$$

The parameters of the average curvature method are shown in Fig. 4.

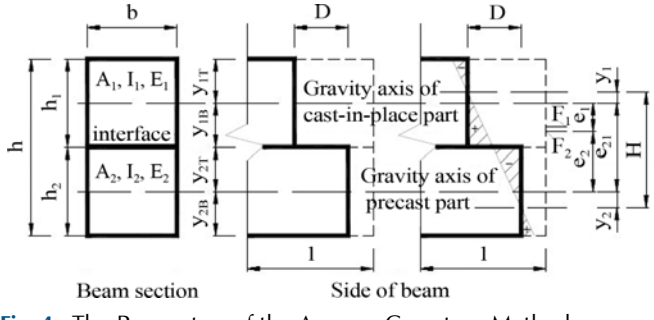

Fig. 4. The Parameters of the Average Curvature Method

θ is the curvature caused by the DSC and can be calculated by

$$\theta = d/H \ , \quad (26)$$

d is also determined by Eq. (15).

2.2.3 Stress Caused by Steel Bars

The steel bars in the concrete restrain the shrinkage and the creep of the concrete, which produces an interaction force. The influence region of the steel bars is divided into two parts as shown in Fig. 5(a).

In region I, the steel bars are distributed uniformly around the concrete. Therefore, the strain of the concrete is considered as the shrinkage and creep strains in the center of the concrete section. According to the force equilibrium as shown in Fig. 5(b), the relationship between the strain of the steel bars and the strain of the concrete is defined as

$$\varepsilon_c E_c A_c = \varepsilon_s E_s A_s \ , \quad (27)$$

$$\varepsilon_c + \varepsilon_s = \varepsilon_{\cosh} + \varepsilon_{coc} \ , \quad (28)$$

where ε_c and ε_s are the tensile strain of the concrete and the compressive strain of the steel bars, respectively; E_c and E_s represent the elastic moduli of the concrete and the steel bars, respectively; A_c and A_s stand for the area of the concrete and the steel bars, respectively; $\varepsilon_{\cosh}$ and ε_{coc} indicate the shrinkage strain and the creep strain in the center of the region, respectively.

$\varepsilon_{\cosh}$ and ε_{coc} are expressed through

$$\varepsilon_{cosh} = \varepsilon_{cosh}(t) - \varepsilon_{cosh}(t_0) \ , \quad (29)$$

$$\varepsilon_{coc} = \varepsilon_{co}(t_0)\varphi_c(t) \ , \quad (30)$$

where $\varepsilon_{cosh}(t)$ and $\varepsilon_{cosh}(t_0)$ are the shrinkage strain of the CIC concrete at the calculation moment and at the loading moment, respectively; $\varepsilon_{co}(t_0)$ represents the strain of the center zone of the concrete at the loading moment; $\varphi_c(t)$ indicates the creep coefficient of the CIC at the calculation moment.

In accordance with Eqs. (27) and (28), ε_c is calculated by

$$\varepsilon_c = \frac{\varepsilon_{cosh} + \varepsilon_{coc}}{1 + 1/(\alpha_{ES}\rho_p)} \ , \quad (31)$$

where α_{ES} is the ratio between the elastic modulus of steel and that of concrete. ρ_p indicates the reinforcement ratio of region I.

In region II, the steel bars are at the bottom of the beam.

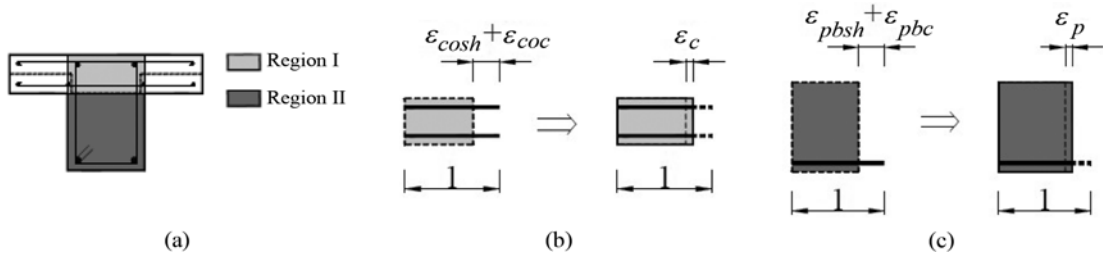

Fig. 5. Tensile Stress on the Concrete Caused by the Steel Bars: (a) Regional Distribution of the Reinforcement Effect on the Concrete, (b) Side View of the Tensile Stress on Region I of the Steel Bars, (c) Side View of the Tensile Stress on Region II of the Steel Bars

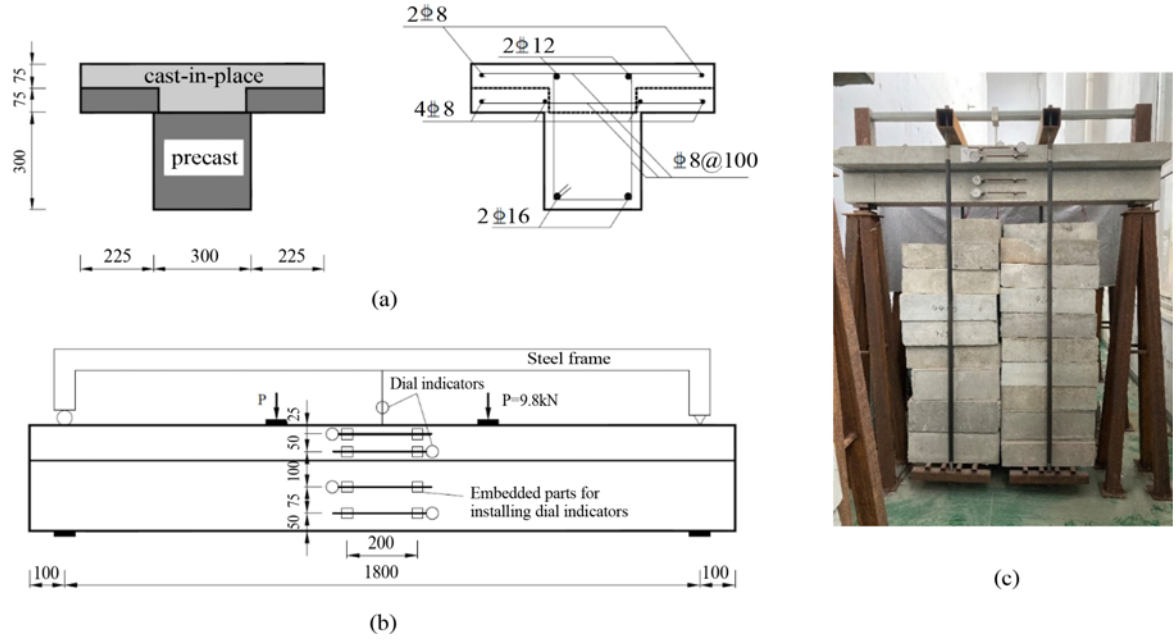

Fig. 6. The Sustained Loading Experiment: (a) Section Dimensions and Reinforcement, (b) Dial Indicator Layout, (c) Experiment Layout

Therefore, the strain of the concrete is considered as the shrinkage strain (ε_{pbsh}) and the creep strain (ε_{pbc}) of the bottom of the beam. Similarly, as shown in Fig. 5(c), the tensile strain of the concrete (ε_p) in region II can be defined as

$$\varepsilon_p = \frac{\varepsilon_{pbsh} + \varepsilon_{pbc}}{1+1/\left(\alpha_{ES}\rho_p\right)}, \tag{32}$$

where ρ_p is the reinforcement ratio of region II.

The tensile stresses on the upper and lower sides of the CIC ($\sigma_{\rho cT}$ and $\sigma_{\rho cB}$) and the PRC ($\sigma_{\rho pT}$ and $\sigma_{\rho pB}$) can be calculated using Eqs. (31) and (32) as follows

$$\sigma_{\rho cT} = \sigma_{\rho cB} = E_c\varepsilon_c, \tag{33}$$

$$\sigma_{\rho pT} = \sigma_{\rho pB} = E_p\varepsilon_p. \tag{34}$$

3. Verification of Theoretical Method

The main purposes of the verification of the developed theoretical method were the validation of the deflection calculation method by a sustained loading experiment and the validation of the stress calculation method by a numerical simulation.

3.1 Sustained Loading Experiment

A sustained loading experiment was carried out according to the section dimensions and the reinforcement of the beam as shown in Fig. 6(a).

The characteristic parameters of the section of the ACCBs were calculated and listed in Table 1, and the loading ages of the PRC and the CIC are presented in Table 2.

The beams were supported by a hinge bearing and a roller bearing, and the length of the beam was 2,000 mm. A pure bending segment with a length of 600 mm was formed under a four-point loading, and the load at each loading point was 9.8 kN. The mix

Table 1. The Characteristic Parameters of the Section of the ACCBs

h_f /mm	h /mm	A_1 /mm	I_1 /10^6 mm^4	y_{1T} /mm	y_{1B} /mm	A_2 /mm	I_1 /10^6 mm^4
150	450	52,061	42.8	49.6	50.4	42,278	145.5
y_{2T} /mm	y_{2B} /mm	e_{21} /mm	e_1 /mm	e_2 /mm	y_1 /mm	y_2 /mm	H /mm
104.04	95.96	154.4	36.4	117.99	22.55	29.16	206

Table 2. The Settings of the Loading Age of the ACCBs

Beam name	L1	L2	L3
Loading age of PRC/d	160	190	210
Loading age of CIC/d	120	150	170

Table 3. The Mix Ratio and Compressive Strength of the Concrete

Type of concrete	Mix ratio of concrete					Compressive strength /MPa
	Cement	Water	Aggregate	Sand	Fly-ash	
PRC	350	100	1,000	820	70	41.95
CIC	370	100	1,000	800	70	57.85

proportion and compressive strength of the concrete are given in Table 3. The reinforcements were ribbed steel bars of Chinese grade HRB400. To avoid disturbance during the measurements, a steel frame was placed on the top of the beam. Moreover, a dial gauge was fixed in the middle of the steel frame to measure the deflection at the mid-span of the composite beam as shown in Fig. 6(b). The layout of the sustained loading experiment is depicted in Fig. 6(c).

3.2 Numerical Simulation Method

The measurement of the long-term stress on the section is quite difficult because the variations in the stress on it is slight. Therefore, a numerical simulation method was proposed for calculating the deflection of and the stress on the ACCBs under shrinkage and creep by utilizing ANSYS software (ANSYS Inc., 2007). In the finite element model, SOLID186 units were used to simulate the concrete, and LINK8 units were employed to simulate the steel bars since the elastic working stage was studied in this case due to the first hypothesis. The geometric and physical parameters of the models were identical to those of the experimental beams. There was no slip between the CIC, the PRC, and the steel bars, and the beam had a mapped grid.

The creep effect was studied by USERCREEP, a user subroutine of ANSYS, and the creep coefficient was determined by the CEB–FIP 90 model (CEB, 1992):

$$\phi(t,t_0)=\phi_0\beta_c(t-t_0), \tag{35}$$

$$\phi_0=\phi_{RH}\beta(f_{cm})\beta(t_0), \tag{36}$$

$$\beta_c(t-t_0)=\left[\frac{(t-t_0)/t_1}{\beta_H+(t-t_0)/t_1}\right]^{0.3}. \tag{37}$$

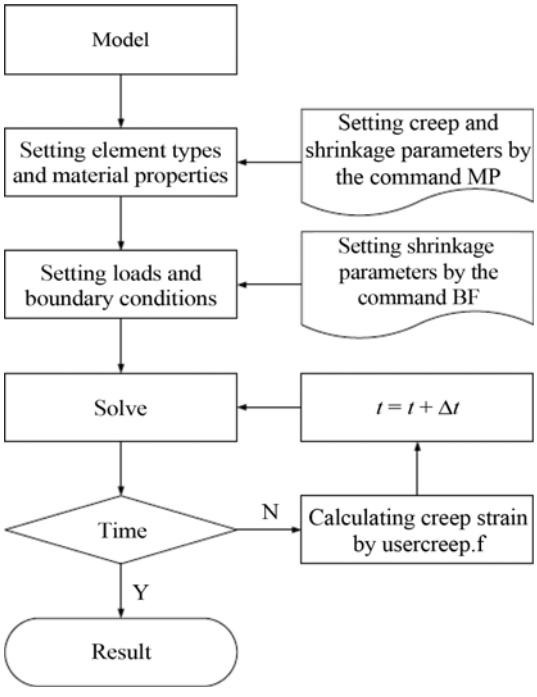

Fig. 7. The Flow Chart of the Numerical Simulation Method

The meaning of the parameters is the same as that described in the model code. The flow chart of the numerical simulation method is shown in Fig. 7.

The equation for updating the creep strain is given by

$$\Delta\varepsilon_c(t)=\frac{\sigma(t)}{E}\cdot\Delta\varphi(t), \tag{38}$$

where $\varepsilon_c(t)$ is the creep strain, and $\varphi(t)$ represents the creep coefficient.

The shrinkage strain was simulated by accounting for the temperature variation and was equivalent to the thermal strain. The temperature field of the whole ACCB was considered to be related to time. The coefficient of linear thermal expansion is calculated by

$$\alpha(t)=\frac{\varepsilon_{sh}(t_0)-\varepsilon_{sh}(t)}{T}, \tag{39}$$

where T represents the temperature; $\varepsilon_{sh}(t_0)$ and $\varepsilon_{sh}(t)$ indicate the shrinkage strain at the loading moment and at the calculation moment respectively and are determined by the CEB–FIP 90 model (CEB, 1992):

$$\varepsilon_{cs}(t,t_s)=\varepsilon_{cso}\beta_s(t-t_s), \tag{40}$$

$$\varepsilon_{cso}=\varepsilon_s(f_{cm})\beta_{RH}, \tag{41}$$

$$\beta_s(t-t_s)=\left[\frac{(t-t_s)/t_1}{350(h/h_o)^2+(t-t_s)/t_1}\right]^{0.5}. \tag{42}$$

The meaning of the parameters is the same as that described in the model code.

This method can be used to calculate the creep strain after the stress–strain redistribution caused by the shrinkage and the creep in each time step.

3.3 Results of Verification

3.3.1 Deflection

The loading moment, the concrete strength, and the creep model were similar in the theoretical method, the experiment, and the numerical simulation. The theoretical, experimental, and numerical data on the coefficients of the deflection creep of the composite beams are plotted in Fig. 8; the coefficients of the deflection creep in Fig. 8 are defined as

$$\varphi=\frac{w-w_0}{w_0}. \tag{43}$$

This figure shows that the results are very close. In fact, for L2 and L3, the difference between the experimental data and the other results is quite small. For L1, the experimental data are marginally smaller than the simulation and theoretical results during most of the holding time but are very close to the other two at a holding time of approximately 365 d.

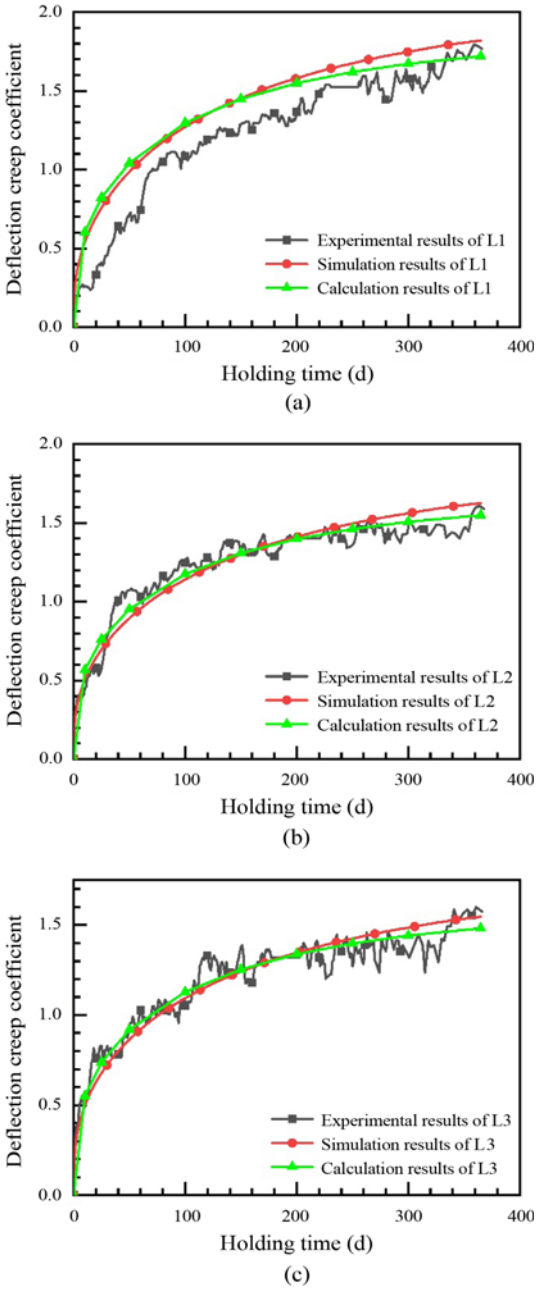

Fig. 8. The Results of the Experiment, the Numerical Simulation, and the Theoretical Calculation: (a) Loading Age of the PRC, 160 d, (b) Loading Age of the PRC, 190 d, (c) Loading Age of the PRC, 210 d

3.3.2 Stress

The mid-span stress on the ACCBs with a CIC loading age of 28 d and a PRC loading age of 68, 98, 128, and 158 d was simulated by the numerical simulation method. The other parameters of the ACCBs were identical to those in Section 3.1. The results of the loading age of 68 d are shown in Fig. 9.

According to Fig. 9, the numerical simulation and the theoretical calculation follow an identical trend. The tensile stress on the bottom of the PRC (σ_{2B}) increases with time, and the compressive stress on the top of the PRC (σ_{2T}) first enlarges but then decreases

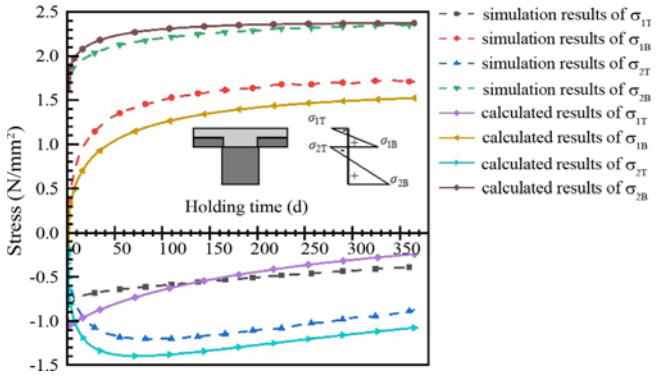

Fig. 9. The Comparison between the Simulated Stress on the Section and the Calculated One

with time. The compressive stress on the bottom of the CIC (σ_{1B}) changes to the tensile stress during the loading and increases with time, while the compressive stress on the top of the CIC (σ_{1T}) declines with time.

The results of the numerical simulation and the theoretical calculation at the other loading ages of the PRC are shown in Fig. 10(a). The difference between the stress on the ACCB determined by the numerical simulation and the one obtained from the theoretical calculation is plotted in Fig. 10(b). This figure demonstrates that the stress difference varies linearly with the loading age of the PRC, which is because the effect of the reinforcement constraint on the concrete reduces the deformation in the numerical simulation. However, in the theoretical calculation, the reinforcement is converted into concrete based on the second hypothesis, and the constraint effect of the reinforcement on the concrete is ignored. The reinforcement produces a tensile strain on the concrete, and the shrinkage strain of the CIC is larger than that of the PRC. Therefore, the tensile strain produced by the reinforcement of the CIC is larger than the strain of the PRC. The ratio of the stress difference to the stress produced by the steel bars in the concrete is plotted in Fig. 10(c). This ratio correlates closely with the loading age. The coefficient of determination (R^2) are 0.99, 0.97, and 0.96. Using the fitting results, Eqs. (33) and (34) are corrected to

$$\sigma_{\rho cT} = \left(0.00479t_{p0} + 0.55226\right)E_c\varepsilon_c, \tag{44}$$

$$\sigma_{\rho cB} = \left(0.00540t_{p0} + 0.82767\right)E_c\varepsilon_c, \tag{45}$$

$$\sigma_{\rho pT} = E_p\varepsilon_p + \left(0.00154t_{p0} + 0.08678\right)E_c\varepsilon_c, \tag{46}$$

$$\sigma_{\rho pB} = E_p\varepsilon_p, \tag{47}$$

where t_{p0} is the loading age of the PRC. The cross-sectional stress on the bottom of the beam (σ_{2B}) calculated by the theoretical method is close to the one determined by the numerical simulation. Therefore, it is not necessary to correct σ_{2B}.

From the verification results, it can be concluded that it is reasonable and feasible to use the theoretical method for calculating the deflection of the ACCB. Although the results of the theoretical calculation are larger than those of the numerical

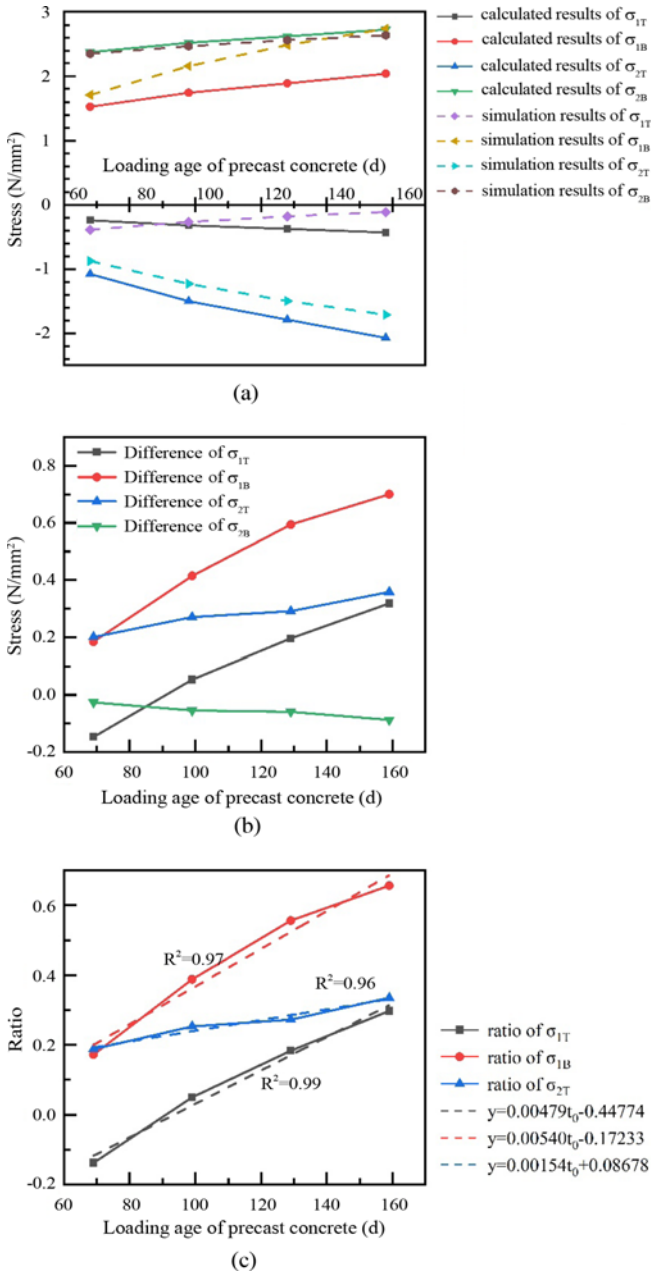

Fig. 10. The Difference between the Results of the Theoretical Method and Those of the Numerical Simulation at the End of a Year: (a) Comparison between the Theoretical Calculation and the Numerical Simulation, (b) Difference between the Theoretical Calculation and the Numerical Simulation at a Holding Time of 365 d, (c) Ratio of the Stress Difference to the Tensile Stress on the Concrete Caused by the Steel Bars

simulation, the difference is within a permissible range and safe for engineering applications. In addition, the theoretical calculation method is convenient for practical engineering.

4. Sensitivity Analysis of Parameters Using Theoretical Calculation Method

This paper presents a practical method for calculating the deflection of and the stress on ACCBs under shrinkage and creep. In addition, this study verifies the effectiveness of the practical method through the experiments and the numerical simulations. There are many design parameters influencing the deflection of or the stress on ACCBs. The parameters closely related to the shrinkage and creep behavior of concrete need to be taken into account. Indeed, because of the development of concrete hydration, concrete is more susceptible to creep at an early age (Criel et al., 2015). The reinforcement in concrete can partly bear the initial stress applied on the concrete, so it restrains the concrete creep (Chen et al., 2020) and benefits the reduction of the creep influence. Furthermore, the drying of the interior of structures depends on the distance from the surface (Maekawa et al., 2011), so the effect of shrinkage and creep is also controlled by the section dimensions and its contact area with the atmosphere. Based on the above analysis, the loading age, the reinforcement ratio, the section dimensions, and the surface area in contact with the atmosphere were selected for the parametric sensitivity analysis of the ACCB.

In order to analyze the sensitivity of the parameters, a case study was carried out. The span of the beam was 3,600 mm, and it had a rectangular cross-section with a width and height of 200 and 400 mm, respectively. The height of the CIC was 120 mm. Also, the uniformly distributed load was 5 kN/m. The cross-section and the reinforcement are shown in Fig. 11. The optimized variables based on the parameters of the ACCBs are listed in Table 4.

The deflection of the ACCB, the stress on the CIC and the PRC, and the stress comparison at a loading time of 365 d were selected for the analysis. The performance of the ACCB with the different loading ages of the PRC, reinforcement ratios, section dimensions, and surface areas in contact with the atmosphere are shown in Figs. 12 – 15, and 17. The meaning of σ_{1T}, σ_{1B}, σ_{2T}, and σ_{2B} is the same as that in Fig. 9. According to GB 50010 (2010), the standard tensile strength—which is the characteristic tensile strength with a confidence level of 95%—of Chinese standard C30 and C35 concrete is 2.01 and 2.20 MPa, respectively. The concrete strength acts as a criterion for judging the risk of cracking.

4.1 Loading Age of PRC

Figure 12 shows the performance of the ACCB at different loading ages.

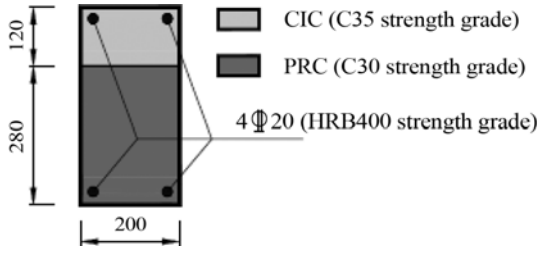

Fig. 11. The Cross-Sectional Parameters of the ACCBs

Table 4. The Parameters of the ACCB with the Optimized Variables

Beam name	Loading age of PRC /d	Width /mm	Height /mm	Height of CIC /mm	Reinforcement ratio /%	Load /kN·m^{-1}
EL1	58	200	400	120	0.79	5
AL2	88	200	400	120	0.79	5
AL3	118	200	400	120	0.79	5
AL3	148	200	400	120	0.79	5
RL2	58	200	400	120	1.18	5
RL3	58	200	400	120	1.57	5
WL2	58	250	400	120	0.79	5
WL3	58	300	400	120	0.79	5
HL2	58	200	450	120	0.79	5
HL3	58	200	500	120	0.79	5

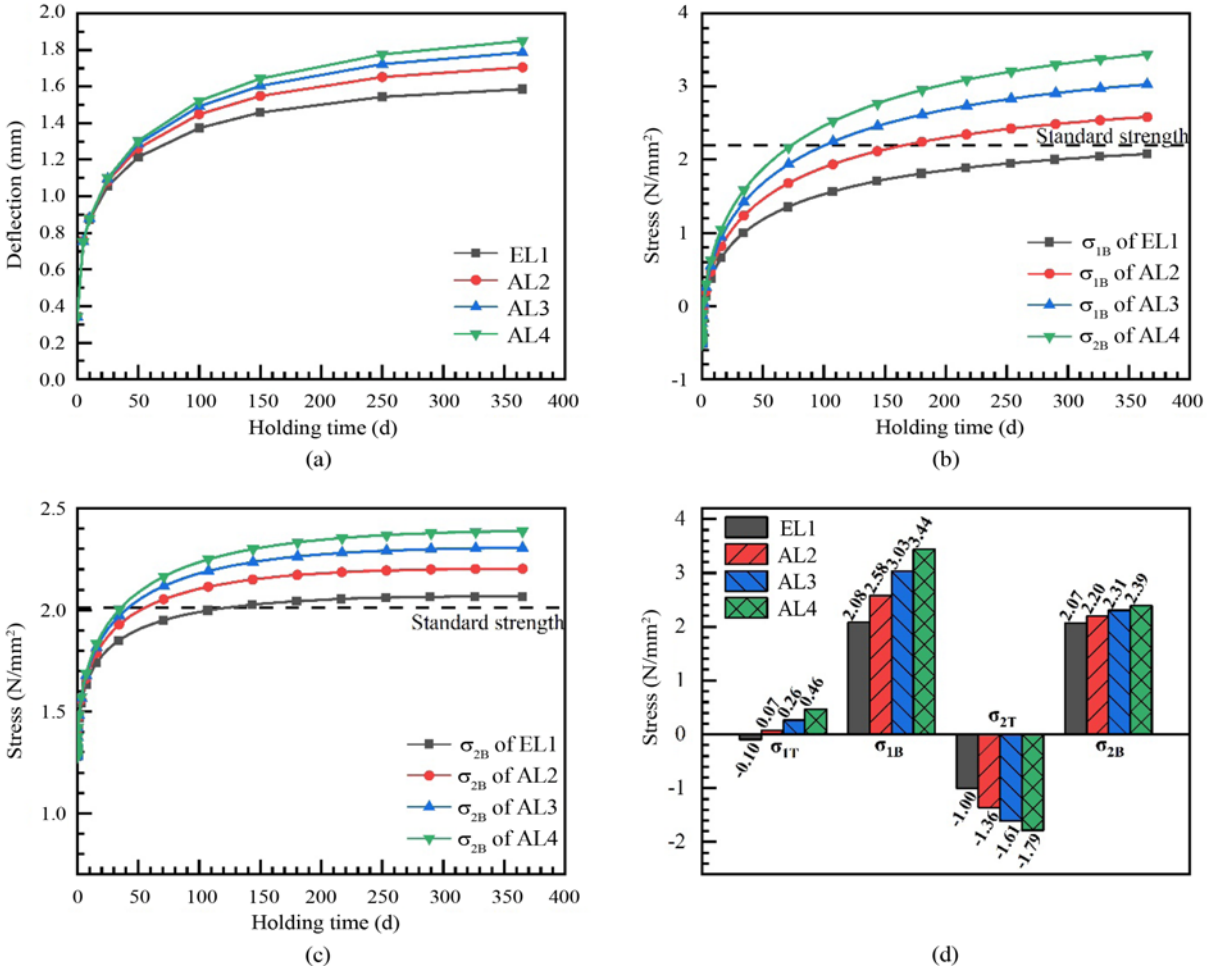

Fig. 12. The Performance of the ACCB at Different Loading Ages: (a) Comparison of the Deflection of the ACCB, (b) Comparison of the Stress of the CIC on the Composite Interface, (c) Comparison of the Stress on the bottom of the Beam, (d) Comparison of the Stress at a Holding Time of 365 d

Figure 12(a) shows the deflection of the ACCB at different loading ages. It is evident that the deflection of the ACCB increases as the loading age of the PRC rises. The PRC with a larger loading age has less shrinkage under the sustained loading. At an identical loading age of the CIC, the ACCB made of the PRC with a smaller loading age has a smaller DSC (both d and D). Thus, the mid-span deflection of the ACCB declines due to the reduction of w_2. Therefore, a reduction in the loading age of the PRC is favorable to the control of the deflection of the ACCB.

The mid-span section stress on the bottom of the CIC and the PRC at the different loading ages is shown in Figs. 12(b) and

12(c), and a comparison between the stress on the top of the beam, on the composite interface, and on the bottom of the beam at a holding time of 365 d is shown in Fig. 12(d).

The variation of the stress indicates that the tensile stress of CIC on the composite interface and on the bottom of the beam increases with time. Moreover, the comparison reveals that the stress on the concrete section increases as the loading age of the PRC extends. This is also caused by a larger DSC. The curvature (θ) is proportional to the DSC (d), and an increase in the DSC enlarges θ and σ_1. Thus, the tensile stress on the ACCB increases with the loading age of the PRC although σ_ρ decreases slightly. The tensile stress on both parts of EL1 is the last to reach the standard strength, which indicates that the tensile concrete in ACCBs with a smaller loading age of the PRC has a smaller failure probability and more time to failure, e.g., cracking. Therefore, to control the section stress, reducing the loading age of the PRC is effective.

4.2 Reinforcement Ratio

Figure 13 shows the performance of the ACCB at different reinforcement ratios.

According to Fig. 13, the deflection of the ACCB at a holding time of 365 d decreases by 3.7% when the reinforcement ratio doubles; the variation of the tensile stress on the PRC also follows the same trend. The stress on the bottom of the beam has a lower growth rate when the reinforcement ratio increases at the preliminary stage of the loading, but it turns to the opposite after a holding time of 140 d. At a loading time of 365 d, the tensile stress on the bottom of the CIC decreases by 0.01%, and the stress on the bottom of the beam enlarges with the increase in the reinforcement ratio. It is evident that a variation in the reinforcement ratio of the tensile reinforcement has a negligible effect on the section stress on the ACCB and a negative effect on the reduction in the failure probability of the tensile concrete; the method of increasing the reinforcement ratio of the tensile reinforcement is less effective and economical.

4.3 Section Dimensions

Figures 14 and 15 depict the comparisons of the deflection of and the section stress on the ACCB with different widths and heights, respectively. It is evident that increasing either the width

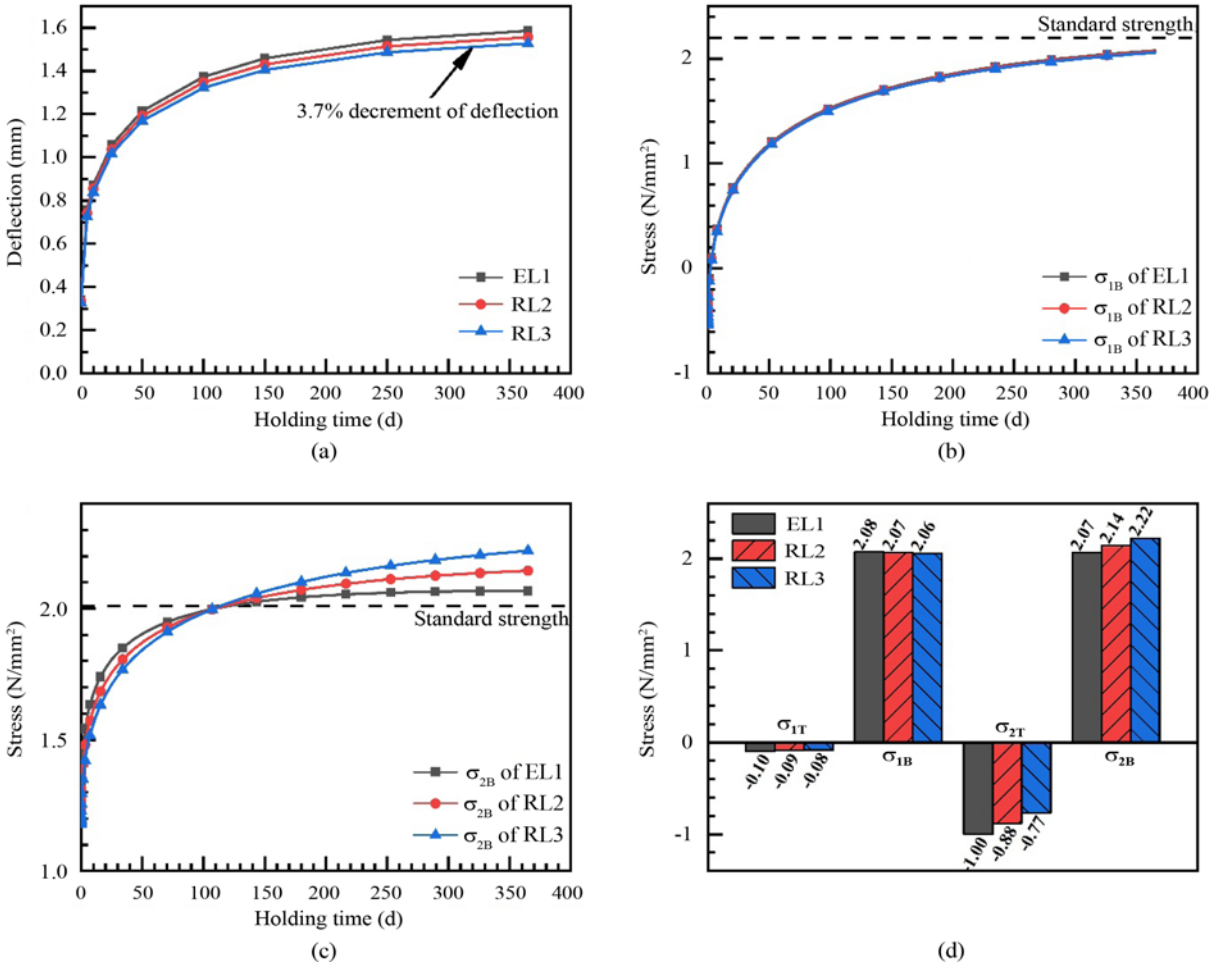

Fig. 13. The Performance of the ACCB at Different Reinforcement Ratios: (a) Comparison of the Deflection of the ACCB, (b) Comparison of the Stress of the CIC on the Composite Interface, (c) Comparison of the Stress on the bottom of the Beam, (d) Comparison of the Stress at a Holding Time of 365 d

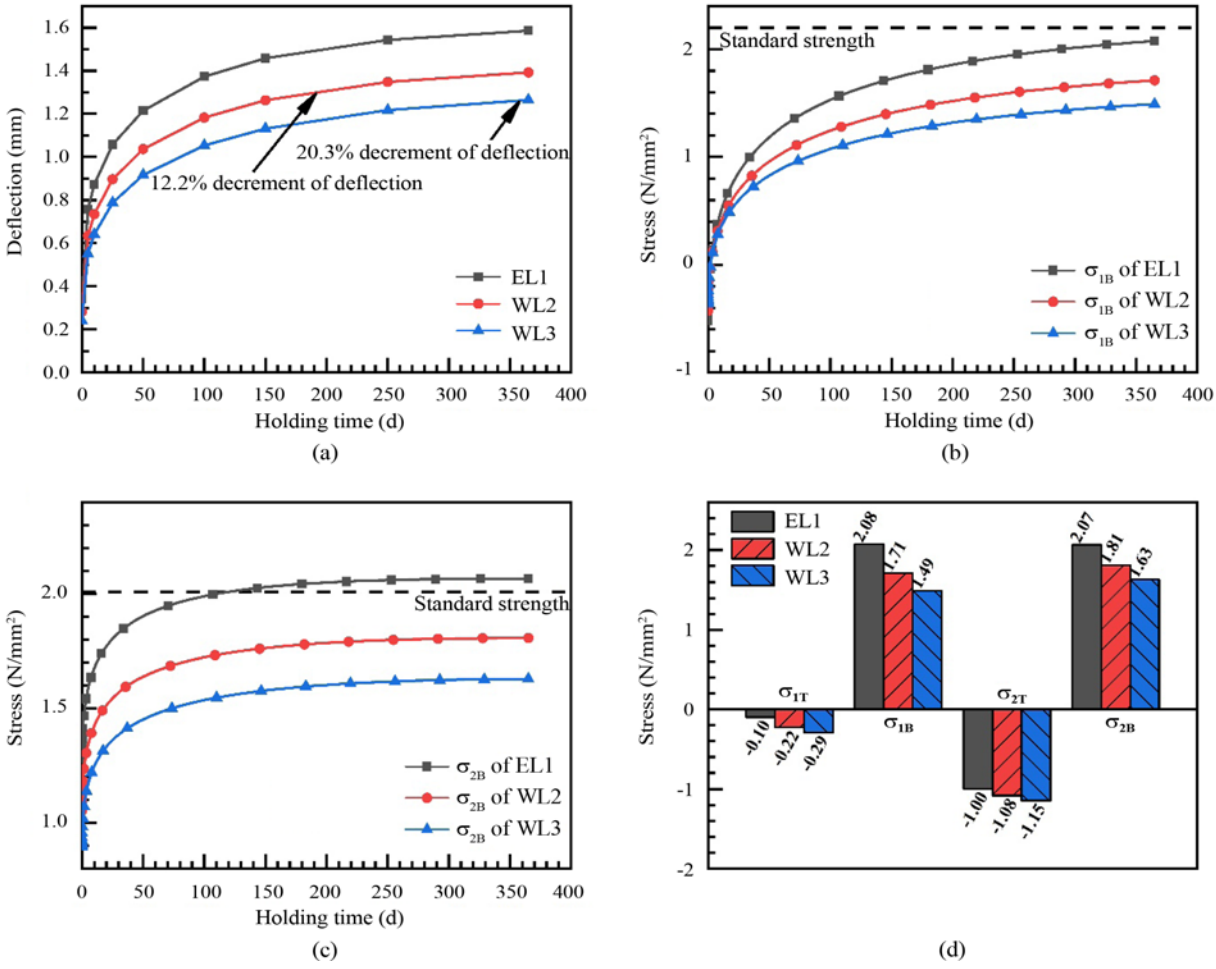

Fig. 14. The Performance of the ACCB at Different Widths of the Beam: (a) Comparison of the Deflection of the ACCB, (b) Comparison of the Stress of the CIC on the Composite Interface, (c) Comparison of the Stress on the Bottom of the Beam, (d) Comparison of the Stress at a Holding Time of 365 d

or the height of the beam is beneficial to the reduction of the deflection of the ACCB under shrinkage and creep. However, increasing the height of the beam has little effect on the reduction of the stress on the bottom of the CIC, while increasing the width of the beam is more effective. As for the stress on the bottom of the beam, both methods are favorable to the reduction of the stress and keep the stress below the standard strength.

According to the above results and analysis, in the design of assembled concrete composite members with shrinkage and creep, the most effective optimization method for reducing the deflection of the ACCB is to increase the height of the beam; the second most effective method is increasing the width of the beam. However, increasing the reinforcement ratio is not suitable for the reduction of the deflection of the ACCB. Additionally, the most effective method for controlling cracks is increasing the width of the beam, followed by increasing its height. However, enlarging the reinforcement ratio is the least effective method of controlling cracks. In addition to the design optimization of the section of the composite beams, the optimization of the loading ages of the PRC in ACCBs is effective.

4.4 Surface Area in Contact with Atmosphere

In addition to the abovementioned variables that affect the deflection of and the section stress on the ACCB, it is obvious that the beams with different positions in the structure have different deflections and section stresses under shrinkage and creep even if they have exactly the same loading age, section dimensions, and reinforcement ratio.

The larger the contact area between the concrete and the atmosphere is, the more apparent the effect of shrinkage and creep becomes. In a structure, there are three main types of contact between the cast-in-place segment and the atmosphere: 1) three faces are in contact with the atmosphere (as in this case). 2) Two faces are in contact with the atmosphere. 3) One face is in contact with the atmosphere. The details are provided in Fig. 16.

EL1 is considered as an example. The curves of the deflection of the beam with time in these three cases are plotted in Figs. 17(a), 17(b), and 17(c). It is clear that as the surface area in contact with the atmosphere decreases, the deflection of the beam declines substantially; this decrease is mainly caused by the reduction of w_2 because w_1 is controlled by the load and the

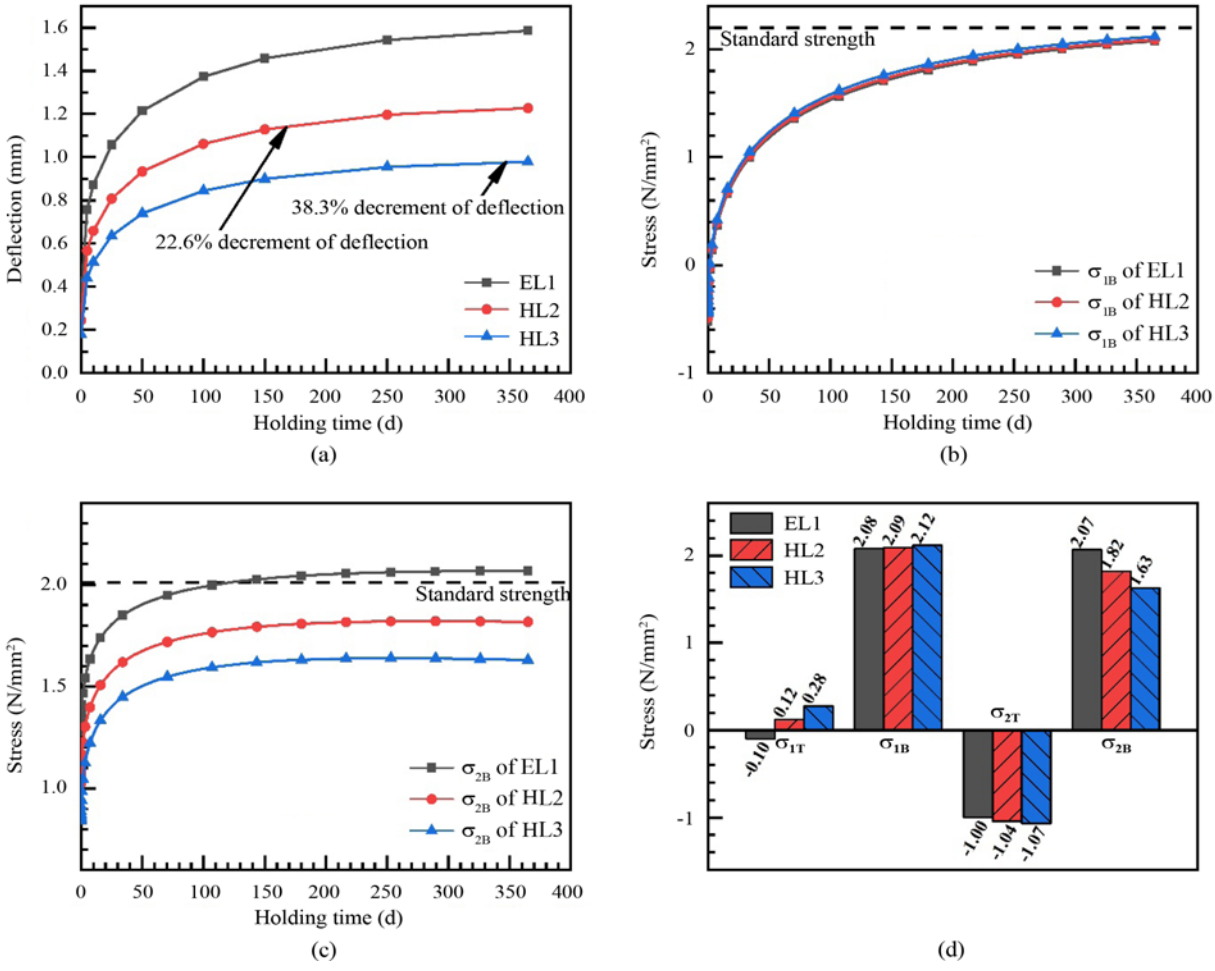

Fig. 15. The Performance of the ACCB at Different Heights of the Beam: (a) Comparison of the Deflection of the ACCB, (b) Comparison of the Stress of the CIC on the Composite Interface, (c) Comparison of the Stress on the Bottom of the Beam, (d) Comparison of the Stress at a Holding Time of 365 d

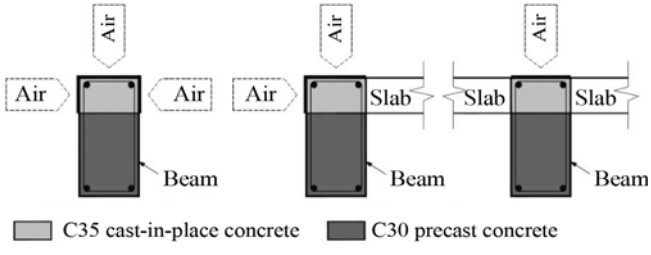

Fig. 16. The Surface Area of the Beam in Contact with the Atmosphere

creep. The decrease in the surface area in contact with the atmosphere reduces the creep coefficient of the CIC from 1.89 to 1.59, a decrease of approximately 0.3. Moreover, the cast-in-place segment exhibits a small stiffness and little influence on the deflection of the beam; therefore, w_1 decreases marginally. On the other hand, w_2 is mainly controlled by the DSC. When the surface area in contact with the atmosphere decreases, the shrinkage strain of the CIC declines, so w_2 decreases. When there is only one contact surface, w_2 decreases to less than zero after a holding time of 200 d as shown in Fig. 17(c) because the shrinkage strain of the CIC (189 με) is smaller than that of the PRC (197 με) during that time. In other words, the DSC reduces the deflection of the beam. In summary, the surface area in contact with the atmosphere mainly affects the variation in w_2.

The cross-sectional stress is calculated as shown in Figs. 17(d), 17(e), 17(f), and 17(g). As the surface area in contact with the atmosphere increases, the tensile stress on the section decreases significantly. This is because the shrinkage strain of the CIC declines with the increase in the surface area in contact with the atmosphere, resulting in the reduction of the differential shrinkage and the tensile stress on the concrete because of the steel bars. Where only one side of the beam is in contact with the atmosphere, the tensile stress on the bottom of the beam and on the CIC is much lower than the standard strength, that is, reducing the surface area in contact with the atmosphere is beneficial to the reduction of the failure probability of the tensile concrete. Compared with the beam of three faces which are in contact with the atmosphere, the tensile stress on the bottom of the beam and on the CIC is reduced by 75.0% and 32.2%, respectively, at a holding time of 365 d. Therefore, reducing the surface area in contact with the atmosphere, for example by

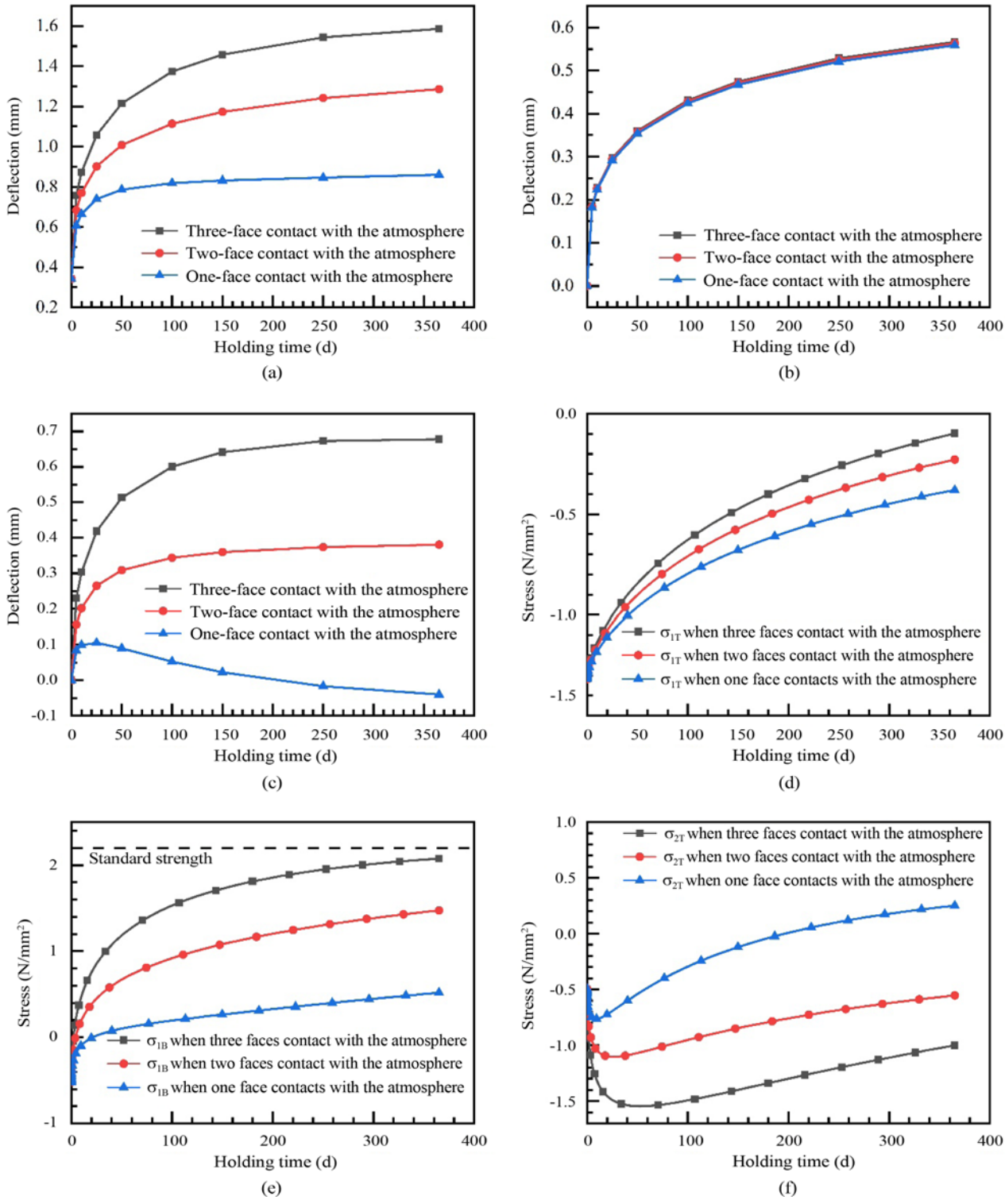

Fig. 17. The Performance of the ACCB with Different Surface Areas in Contact with the Atmosphere: (a) Comparison of the Total Deflection of the Beam, (b) Comparison of Deflection w_1, (c) Comparison of Deflection w_2, (d) Comparison of the Stress on the top of the Beam, (e) Comparison of the Stress of the CIC on the Composite Interface, (f) Comparison of the Stress of the PRC on the Composite Interface

changing the position of the assembled concrete composite members, is favorable to controlling of the section stress and is considered as an effective optimization method for the design of assembled concrete composite members when considering shrinkage and creep. In addition, an atmospheric contact area with some special conditions such as a high-humidity environment is also more beneficial to the reduction in the deflection of and the stress on the beam than the natural environment (Huang et al., 2020).

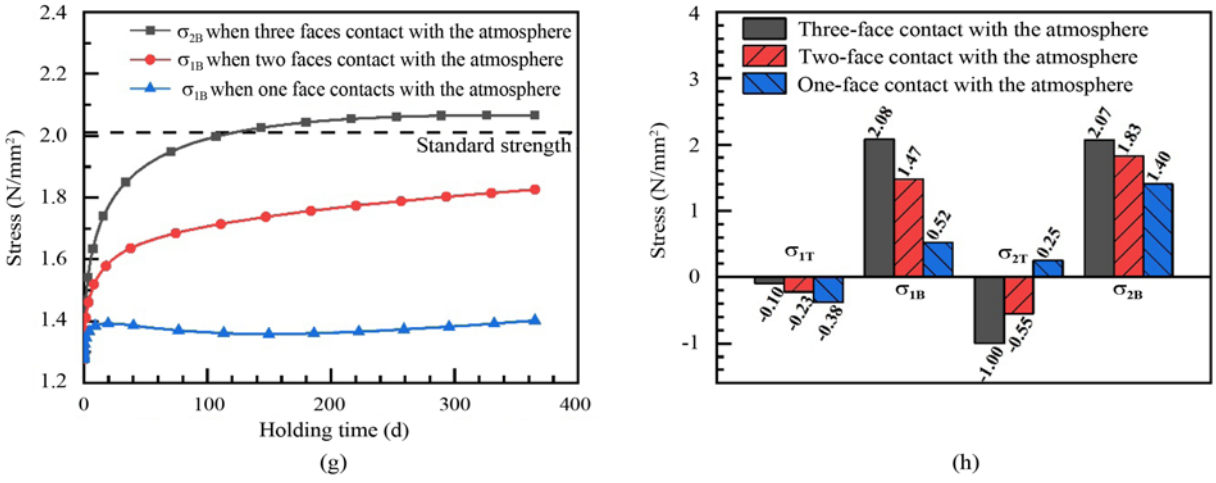

Fig. 17. (continued): (g) Comparison of the Stress on the Bottom of the Beam, (h) Comparison of the Stress at a Holding Time of 365 d

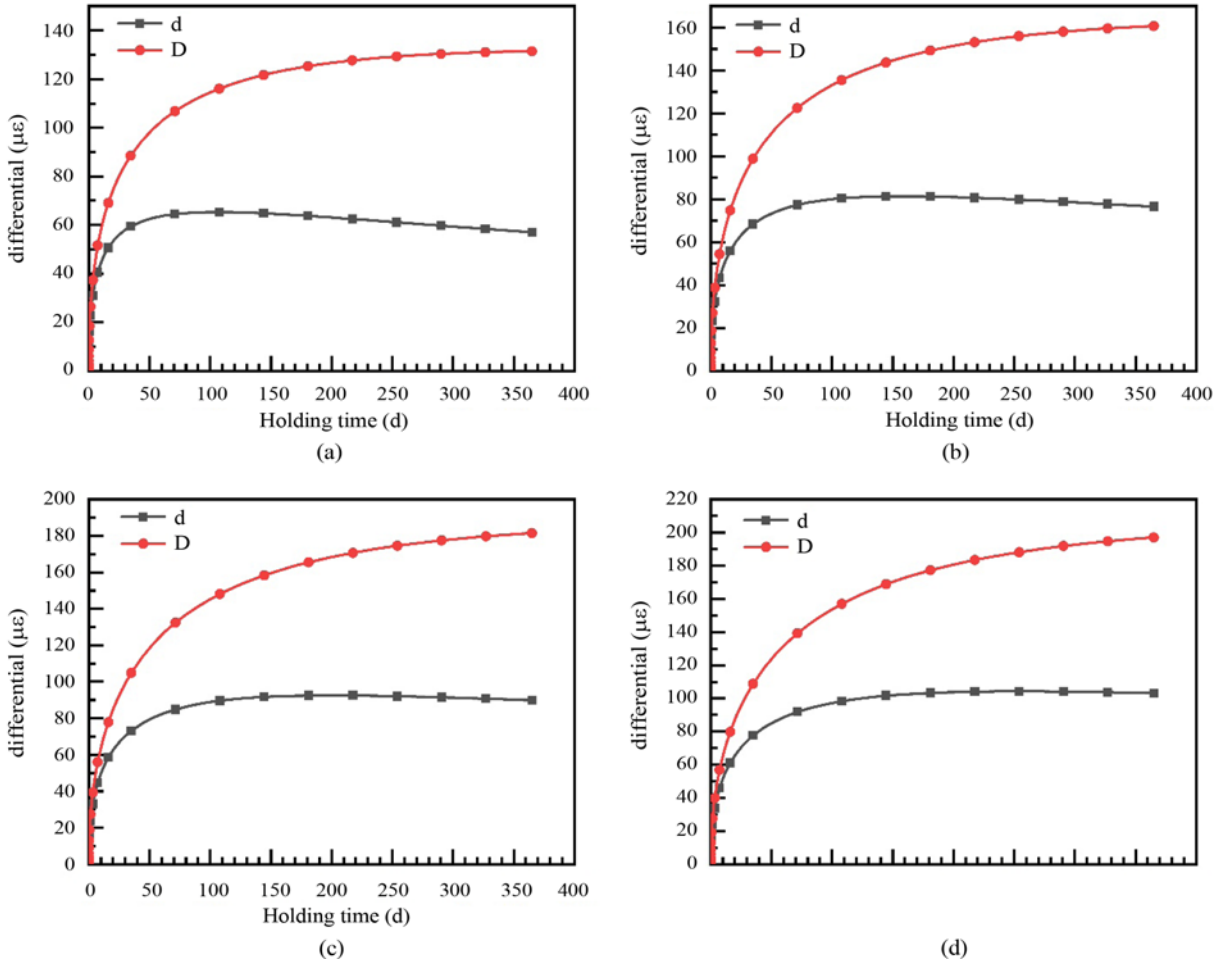

Fig. 18. The Actual DSC at the Composite Interface of the ACCB at a Loading Age of: (a) 68 d, (b) 98 d, (c) 128 d, (d) 158 d

Therefore, if a large surface area in contact with the atmosphere cannot be avoided or the position of the beam cannot be changed, wet curing measures can be taken to reduce the contact area of the member with the atmosphere.

5. Optimization Design Framework Based on Theoretical Calculation Method

The effects of shrinkage and creep are rarely considered in the design of assembled members. The calculation method proposed in this

paper can be utilized to optimize the design of assembled members by considering the effects of shrinkage and creep so as to prevent problems caused by shrinkage and creep such as concrete cracking.

5.1 Simplification of Theoretical Calculation Method

The actual DSC cannot be determined directly by a simple mathematical operation, and it needs to be calculated with the assistance of MATLAB software according to Eq. (15), which is not convenient for optimization design. Thus, the feasibility of the simplification is discussed in this context.

As for the case in Section 3.2, the calculation results of d are shown in Fig. 18.

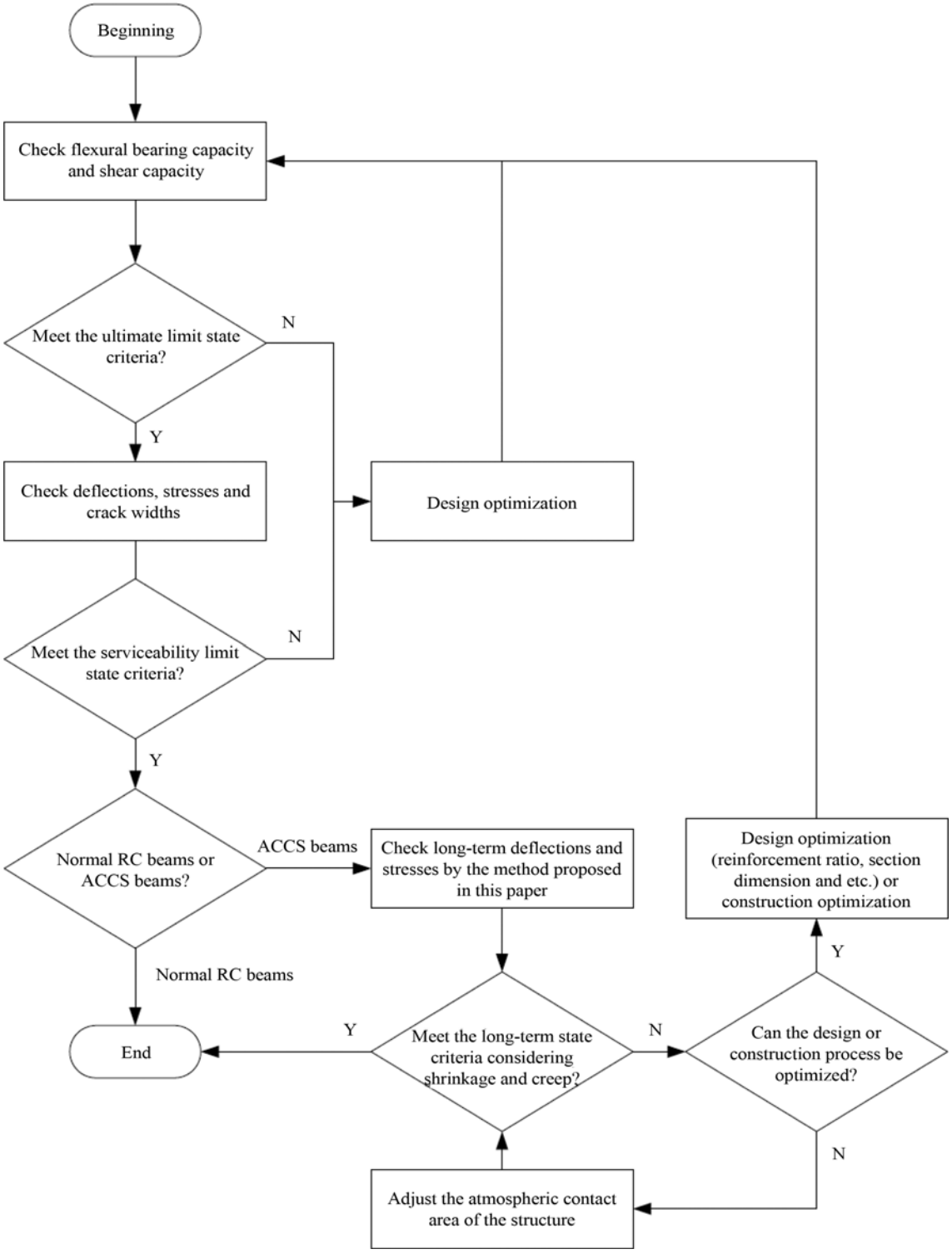

Fig. 19. The Framework for the Review and Optimization of the Reinforced Concrete Structures

Table 5. Review Results of the Beam AL2 before and after Three Optimizations

Checked items		Before optimization	OM 1	OM 2	OM 3
Items of ultimate limit state	Flexural bearing capacity/kN·m^{-1}	47.6	47.6	48.6	48.6
	Shear capacity/kN·m^{-1}	43.0	43.0	53.8	53.8
Items of serviceability limit state	Deflection/mm	0.34	0.34	0.28	0.28
	Stress at the bottom of CIC/MPa	-0.52	-0.52	-0.43	-0.43
	Cracks at the bottom of CIC	×	×	×	×
Items of long-term state (at 365 d holding time)	Deflection/mm	1.71	1.59	1.52	1.39
	Stress at the bottom of CIC/MPa	2.58	2.08	1.82	1.71
	Cracks at the bottom of CIC	√	×	×	×

Two meaningful results can be concluded: First, d is significantly smaller than D. Second, the concrete creep reduces the DSC substantially, which is favorable to the reduction of the cross-section stress on the beam. Especially, for the beams with a smaller loading age of the PRC such as 68 and 98 d, the changing trend becomes descending, and the difference between d and D enlarges. Therefore, using the actual DSC, rather than D, for calculating σ_1 is more accurate because of the proportional relationship between σ_1 and the DSC. Also, it is necessary to determine the actual DSC in the calculation of the section stress on the beam.

However, the calculation of the deflection of the beam is different. Comparing Eqs. (4) with (20) demonstrates that the proportion of the difference between d and D in w_2 is relatively small. In this case, the difference between corrected w_2 (calculated by Eq. (20)) and uncorrected w_2 (calculated by Eq. (4)) is less than 2% in the calculation of the deflection of the beam; hence, the accuracy of using Eq. (4) for practical design is acceptable. Therefore, Eq. (4) can be used as a simple formula to calculate the deflection of the ACCBs without determining the actual DSC with the assistance of MATLAB software.

5.2 Framework of Design Optimization

The design processes of normal reinforced concrete components include the section design based on the ultimate bearing capacity limit state and the section review based on the serviceability limit state. Due to the effects of shrinkage and creep, the risk of the additional deflections or unexpected cracking of the ACCS should be checked. The review or optimization of the ACCB can be carried out by utilizing the theoretical method developed herein. In this context, the framework is proposed in Fig. 19.

For an ACCB, after the ultimate bearing capacity limit state and the serviceability limit state fulfill the requirements, the long-term deflection of and the stress on the beam need to be calculated by the method proposed above. If the long-term state cannot satisfy the requirements, the design optimization such as the optimization of the section dimensions or the optimization of the construction process should be applied. If the construction of the structure is completed or the structure cannot be optimized due to other reasons, the surface area in contact with the atmosphere can be reduced to satisfy the requirements.

A case study is carried out for the review or optimization of ACCBs. The optimization of beam AL2 in Section 4 is discussed. The design parameters of the beam are identical to those in Fig. 11 and Table 4. The beam is also under a uniformly distributed load of 5 kN/m. The mid-span deflection of and stresses on the beam under shrinkage and creep are shown in Fig. 12. It can be learned from Figs. 12(b) and 12(d) that the stress of CIC on the interface is larger than the standard tensile strength. It means the concrete at that position would probably crack after 365 d holding time. Therefore, it's necessary to propose a design optimization or construction optimization for the beam if cracking is not allowed during operation.

Three different possible optimization methods (OM) are proposed according to the results of sensitivity analysis in Section 4. OM1 is to reduce the loading age of PRC from 88 d to 58 d. OM2 is to enlarge the width of the beam from 200 mm to 250 mm. OM3 is the combination of OM1 and OM2 (58 d PRC loading age and 250 mm beam width). Following the framework in Fig. 19, the review results of the beam before and after optimizations are shown in Table 5. The calculation of items of ultimate limit state is according to GB 50010 (2010).

Table 5 shows that the beam AL2 meet the requirements of serviceability limit state. However, cracks appear during sustained loading period. And all the three optimizations could avoid the appearance of cracks because the long-term stresses at that position have reduced below the tensile strength of concrete (2.20 MPa). The long-term deflection has also decreased. In addition, the comparation of the three optimizations indicates that combinations of two or more optimizations would be more beneficial for the long-term performance of ACCBs. There are no decreases appearing in items of ultimate limit state and the serviceability after optimizing. This case study indicates that optimization based on long-term state is objectively necessary, and also the proposed framework is effective.

6. Conclusions

An assembled concrete composite structure contains a large number of concrete bonding interfaces. The different shrinkage and creep behaviors of the old and new concrete can pose the risk of the additional deflections or unexpected cracking of the

ACCS. The traditional structural design neglects the section review or section optimization process considering the DSC. Thus, a theoretical calculation method based on the mean curvature method is proposed herein. Although the long-term deflections of and section stresses on the beam can be calculated by FEM, a simpler theoretical method is needed in the process of design. The accuracy of the developed method is verified by the experimentation and the numerical simulation. Also, the feasibility of the simplification of the theoretical method is discussed at the end.

The results of the parametric sensitivity analysis can be helpful for designers to select the best approaches for optimization. The optimization of the section dimensions is the most effective way to reduce the deflection of the beam and control the risk of cracking through the discussed ways. In addition to the design optimization of the section dimensions of the assembled concrete composite beam, the selection of a reasonable loading time is effective. Another interesting finding of this work is that the surface area of the CIC in contact with the atmosphere is favorable for reducing the deflection of the beam and for controlling the section stress on the beam. This indicates that the beams in various positions in the structure perform differently.

An optimization design framework based on the theoretical calculation method is proposed at the end of this work. The section review or the section optimization considering shrinkage and creep is added into the traditional section design process. The framework demonstrates that the section review or the section optimization is quite convenient and effective. This process can helpfully be employed to control the risk of the additional deflections or cracking of the assembled concrete composite beams during the long-term operation of buildings.

The research has some limitations. The actual DSC needs to be determined with the assistance of MATLAB software and could not be simplified by replacing with D in the calculation of section stresses. Checking tables of the actual DSC could be made for some typical sections with common load cases in future studies, which would probably simplify the calculation.

In the future, calculation method of deflection of and stress on ACCBs with other constraints would be studied. The long-term performance of cantilever ACCBs and clamped ACCBs is also worth studying and discussing. Since the behavior of cantilever beams could be considered as a reverse bending to simply supported beams, and the clamped beams could be considered as a combination of simply supported beams and cantilever beams, the approach for the development of the calculation method in Section 2 could be also adopted with some further analysis. Thus, the design optimization framework would be further improved.

Acknowledgments

The research was financially supported by National Key R&D Program of China (2016YFC0701400); the National Natural Science Foundation of China (51820105012, 51878610, and 51638013); and the Natural Science Foundation of Zhejiang Province (LY18E080003 and LQ19E080011).

ORCID

Jianghong Mao https://orcid.org/0000-0002-0686-418X

References

ACI Committee 209 (1982) Prediction of creep, shrinkage and temperature effects in concrete structures. American Concrete Institute, Farmington Hills, MI, USA

ANSYS Inc. (2007) Guide to ANSYS user programmable features. Release 11.0, Canonsburg, PA, USA

Ban H, Uy B, Pathirana SW, Henderson I, Mirza O, Zhu X (2015) Time-dependent behavior of composite beams with blind bolts under sustained loads. *Journal of Constructional Steel Research* 112:196-207, DOI: 10.1016/j.jcsr.2015.05.004

Bažant ZP, Bweja S (1995) Creep and shrinkage prediction model for analysis and design of concrete structures: Model B3. *Materials and Structures* 28:357-365, DOI: 10.1007/bf02473152

Bertagnoli G, Gino D, Martinelli E (2017) A simplified method for predicting early-age stresses in slabs of steel-concrete composite beams in partial interaction. *Engineering Structures* 140:286-297, DOI: 10.1016/j.engstruct.2017.02.058

Beushausen H (2016) A parameter study on the age at cracking of bonded concrete overlays subjected to restrained shrinkage. *Materials and Structures* 49:1905-1916, DOI: 10.1617/s11527-015-0622-6

Cas B, Planinc I, Schnabl S (2018) Analytical solution of three-dimensional two-layer composite beam with interlayer slips. *Engineering Structures* 173:269-282, DOI: 10.1016/j.engstruct.2018.06.108

CEB (1992) CEB–FIP model code 90. Thomas Telford, London, UK, DOI: 10.1680/ceb-fipmc1990.35430.0002

Chen X (1981) An experimental research on the differential shrinkage and creep of simply supported rectangular prestressed concrete composite beams. *Journal of Wuhan University of Technology* 04:55-84 (in Chinese)

Chen S, Yan W, Gao J (2012) Experimental investigation on the seismic performance of large-scale interior beam-column joints with composite slab. *Advances in Structural Engineering* 15:1227-1237, DOI: 10.1260/1369-4332.15.7.1227

Chen A, Yossef M (2016) Analytical model for deck-on-girder composite beam system with partial composite action. *Journal of Engineering Mechanics* 142, DOI: 10.1061/(ASCE)EM.1943-7889.0000991

Chen P, Zhou X, Zheng W, Wang Y, Bao B (2020) Influence of high sustained loads and longitudinal reinforcement on long-term deformation of reinforced concrete beams. *Journal of Building Engineering* 30, DOI: 10.1016/j.jobe.2020.101241

Chiang Y, Chan EH, Lok LK (2006) Prefabrication and barriers to entry – A case study of public housing and institutional buildings in Hong Kong. *Habitat International* 30:482-499, DOI: 10.1016/j.habitatint.2004.12.004

Cosenza E, Pecce M (2001) Shear and normal stresses interaction in coupled structural systems. *Journal of Structural Engineering* 127:84-88, DOI: 10.1061/(asce)0733-9445(2001)127:1(84)

Criel P, Caspeele R, Matthys S, Taerwe L, Furuta H (2015) Creep experiments and analysis of T-shaped beams subjected to loading and unloading at young age. CRC Press, Boca Raton, FL, USA, 2186-2192

Cyron W, Nilsson M, Emborg M, Ohlsson U (2019) Bonded concrete overlays: A brief discussion on restrained shrinkage deformations

and their prediction models. *Nordic Concrete Research* 61:107-129, DOI: 10.2478/ncr-2019-0019

Ecsedi I, Baksa A (2016) Analytical solution for layered composite beams with partial shear interaction based on Timoshenko beam theory. *Engineering Structures* 115:107-117, DOI: 10.1016/j.engstruct.2016.02.034

Erkmen RE, Bradford MA (2011) Time-dependent creep and shrinkage analysis of composite beams curved in-plan. *Computers & Structures* 89:67-77, DOI: 10.1016/j.compstruc.2010.08.004

Fan J, Feng D, Wu G, Hou S, Lu Y (2020) Experimental study of prefabricated RC column-foundation assemblies with two different connection methods and using large-diameter reinforcing bars. *Engineering Structures* 205, DOI: 10.1016/j.engstruct.2019.110075

Gardner NJ, Lockman MJ (2001) Design provisions for drying shrinkage and creep of normal-strength concrete. *ACI Materials Journal* 98:159-167, DOI: 10.14359/10199

GB50010 (2010) Code for design of concrete structures. GB50010, China Architecture and Building Press, Beijing, China (in Chinese)

Gillum AJ, Shahrooz BM, Cole JR (2001) Bond strength between sealed bridge decks and concrete overlays. *ACI Structural Journal* 98:872-879, DOI: 10.14359/10754

Gohnert M (2000) Proposed theory to determine the horizontal shear between composite precast and in situ concrete. *Cement & Concrete Composites* 22:469-476, DOI: 10.1016/S0958-9465(00)00050-0

Halicka A (2011) Influence new-to-old concrete interface qualities on the behavior of support zones of composite concrete beams. *Construction and Building Materials* 25:4072-4078, DOI: 10.1016/j.conbuildmat.2011.04.045

Han CX, Lan SW, Yao KC, Zhang J (2019) Numerical analysis of key influences factors of creep and shrinkage performance of composite beams. International conference on civil, architecture and disaster prevention, October 19-21, Hefei, China, DOI: 10.1088/1755-1315/218/1/012047

Hong J, Shen GQ, Li Z, Zhang B, Zhang W (2018) Barriers to promoting prefabricated construction in China: A cost-benefit analysis. *Journal of Cleaner Production* 172:649-660, DOI: 10.1016/j.jclepro.2017.10.171

Hu X, Xue W, Qi D (2020) Experimental studies on precast post-tensioned concrete connections with composite beams and multi-story columns. *Magazine of Concrete Research* 72:1260-1275, DOI: 10.1680/jmacr.18.00595

Huang D, Wei J, Liu X, Du Y, Zhang S (2019a) Experimental study on influence of post-pouring joint on long-term performance of steel-concrete composite beam. *Engineering Structures* 186:121-130, DOI: 10.1016/j. engstruct.2019.02.003

Huang D, Wei J, Liu X, Xiang P, Zhang S (2019b) Experimental study on long-term performance of steel-concrete composite bridge with an assembled concrete deck. *Construction and Building Materials* 214:606-618, DOI: 10.1016/j.conbuildmat.2019.04.167

Huang Y, Zhou Y, Liu Y, Xiao L (2020) Tensile creep tests of hydraulic concrete under different curing conditions. *Journal of Materials in Civil Engineering* 32(4), DOI: 10.1061/(ASCE)MT.1943-5533.0003090

Jung Y, Lin W, Hao H, Cho YH (2017) Interface behavior of partial depth repair for airport concrete pavement subjected to differential volume change. *Construction and Building Materials* 143:515-521, DOI: 10.1016/j.conbuildmat.2017.03.161

Khan I, Castel A, Gilbert RI (2017) Tensile creep and early-age concrete cracking due to restrained shrinkage. *Construction and Building Materials* 149:705-715, DOI: 10.1016/j.conbuildmat.2017.05.081

Khoo JH, Li B, Yip WK (2006) Tests on precast concrete frames with connections constructed away from column faces. *ACI Structural Journal* 103:18-27, DOI: 10.14359/15082

Kurama YC, Sritharan S, Fleischman RB, Restrepo JI, Henry RS, Ghosh SK, Bonelli P (2018) Seismic-resistant precast concrete structures: State of the art. *Journal of Structural Engineering* 144:3118001, DOI: 10.1061/(ASCE)ST.1943-541X.0001972

Lam SSE, Wong V, Lee RSM (2019) Bonding assessment of semi-precast slabs subjected to flexural load and differential shrinkage. *Engineering Structures* 187:25-33, DOI: 10.1016/j.engstruct.2019.02.029

Liu X, Bradford MA, Chen Q, Ban H (2016) Finite element modelling of steel-concrete composite beams with high-strength friction-grip bolt shear connectors. *Finite Elements in Analysis and Design* 108:54-65, DOI: 10.1016/j.finel.2015.09.004

Liu X, Erkmen RE, Bradford MA (2012) Creep and shrinkage analysis of curved composite beams with partial interaction. *International Journal of Mechanical Sciences* 58:57-68, DOI: 10.1016/j.ijmecsci.2012.03.001

Long G, Xie Y, Ding W, Omran A (2014) Ion-transport characteristics of new-old concrete composite system. *Journal of Central South University* 21:790-798, DOI: 10.1007/s11771-014-2002-8

Maekawa K, Chijiwa N, Ishida T (2011) Long-term deformational simulation of PC bridges based on the thermo-hygro model of micro-pores in cementitious composites. *Cement and Concrete Research* 41:1310-1319, DOI: 10.1016/j.cemconres.2011.03.021

Magnucki K, Lewinski J, Magnucka-Blandzi E (2020) Bending of two-layer beams under uniformly distributed load - Analytical and numerical FEM studies. *Composite Structures* 235, DOI: 10.1016/j.compstruct.2019.111777

Martinelli E (2021) A general numerical model for simulating the long-term response of two-layer composite systems in partial interaction. *Composite Structures* 257, DOI: 10.1016/j.compstruct.2020.112929

Morenoa JA, Tamayo JLP, Morsch IB, Miranda MP, Reginato LH (2019) Statistical bias indicators for the long-term displacement of steel-concrete composite beams. *Computers and Concrete* 24:379-397, DOI: 10.12989/cac.2019.24.4.379

Orta L, Bartlett FM (2020) Sensitivity analysis of restrained shrinkage stresses of concrete deck overlays. *Engineering Structures* 210, DOI: 10.1016/j.engstruct.2020.110396

Ranzi G, Bradford M (2006) Analytical solutions for the time-dependent behavior of composite beams with partial interaction. *International Journal of Solids and Structures* 43:3770-3793, DOI: 10.1016/j.ijsolstr.2005.03.032

Schnabl S, Saje M, Turk G, Planinc I (2007) Analytical solution of two-layer beam taking into account interlayer slip and shear deformation. *Journal of Structural Engineering* 133:886-894, DOI: 10.1061/(asce)0733-9445(2007)133:6(886)

Si XT, Au FTK (2011) An efficient method for time-dependent analysis of composite beams. *Procedia Engineering* 14:1863-1870, DOI: 10.1016/j.proeng.2011.07.234

Xue W, Hu X, Yang Y (2019) Full-scale tests on composite concrete T-beams subjected to cyclic and monotonic loading. *Proceedings of the Institution of Civil Engineers-Structures and Buildings* 172:671-684, DOI: 10.1680/jstbu.17.00174

Xue W, Yang X, Hu X (2020) Full-scale tests of precast concrete beam-column connections with composite T-beams and cast-in-place columns subjected to cyclic loading. *Structural Concrete* 21:169-183, DOI: 10.1002/suco.201800171

Zhu H, Hu Y, Li Q, Ma R (2020) Restrained cracking failure behavior of concrete due to temperature and shrinkage. *Construction and Building Materials* 244, DOI: 10.1016/j.conbuildmat.2020.118318